Supporting Information

SI Materials and Methods

Cloning of *Mmα*-GluII

Amplification of the *Mus musculus ganab* (isoform 2) and *prkcsh* genes (UniProt Accession numbers: Q8BHN3-2 and O08795) was achieved by polymerase chain reaction (PCR) using a standard Phusion Flash ThermoFisher Scientific) protocol and the primers: *ganab* Forward 5'-GCGTAGCTGAAACCGGCGCTGTGGATAGAA 3', Reverse 5'-GGTGGCTCCAGCTAGCTCGAAGATGAATACTCCAGTCGGATGC-3' and *prkcsh* Forward 5'-GCGTAGCTGAAACCGGCGCTGTAGAAGTTAAGAGACCCCGGGG-3', Reverse 5'-GTGATGGTGATGTTTGT 3'. A DpnI digestion was performed to prevent template DNA from contaminating the newly assembled product. Purification of the PCR products was achieved by AMPure XP magnetic beads (Beckman Coulter) following the manufacturer's protocol. Assembly of the constructs was carried out by mixing 1 µl of the linearized vector (pOPINGS and pOPING for *ganab* and *prkcsh*, respectively, provided by the Oxford Protein Production Facility) with 5 µl of the purified PCR product to a total volume of 10 µl and added to lyophilized In-Fusion HD EcoDry enzyme mix (Clontech). pOPINGS bears C-terminal Strep-II and hexahistidine tags and pOPING bears a C-terminal hexahistidine tag. After the assembly reaction at 42 ºC for 30 min, transformation was carried out in One Shot OmniMAX 2 Chemically Competent *E. coli* (Life Technologies) following the manufacturer's protocol. Correctly assembled colonies were screened by blue-white selection and the plasmids were isolated.

Cloning of *Mmα*-GluII point mutants

Site-directed mutagenesis was carried out on the wild-type *ganab* template present in Litmus28i (New England Biolabs) using the Q5 Site-Direct Mutagenesis kit (New England Biolabs) according to the manufacturer's protocol. Subcloning into the pHLsec expression vector of correctly identified mutants was then carried out using the above strategy.

Expression of *Mmα*-GluII

Co-transfection into the FreeStyle 293 Expression System (Life Technologies) was carried out according to the manufacturer's protocol. The transfection reagent was used at 0.125% v/v of the culture volume. The plasmids were used in equimolar amounts at a total of 0.1% w/v of the culture volume. Cells were maintained at 37 ºC, 5 % CO_2 and 135 rpm.

Purification of *Mmα*-GluII

After 4 days the cells were harvested by centrifugation at 3000 g for 15 min. The supernatant was adjusted to 1xPBS and 5 mM imidazole. 10 M NaOH was used to bring the pH to 7.5. The supernatant was flowed through a 5 ml HisTrap excel (GE LifeSciences) column and washed with 10 column volumes 40 mM imidazole in PBS supplemented with 5% w/v glycerol. The protein was eluted with 10 column volumes of 400 mM imidazole in PBS supplemented with 5% w/v glycerol. The imidazole was removed from the eluate by dialysis into Strep Wash Buffer (100 mM Tris pH 8.0, 150

mM NaCl, 1 mM EDTA). The *Mm*α-GluII was bound to 10 ml of StrepTactin Superflow High Capacity resin (IBA). The resin was washed with 3 column volumes of the Strep Wash Buffer followed by 3 column volumes of Strep Elution Buffer (100 mM Tris pH 8.0, 150 mM NaCl, 1 mM EDTA, 2.5 mM D-desthiobiotin). The pooled fractions were concentrated with 30 kDa MWCO Amicon Ultra-15 Ultrafiltration devices (Millipore). The concentrated enzyme was applied to a Superdex 200 16/600 column (GE Lifesciences) in 20 mM HEPES pH 7.5, 150 mM NaCl. The appropriate fractions were pooled and concentrated as above. Yield of the full-length *Mm*α-GluII is 8mg/L of culture. Expression and purification of the point mutants was carried out in an identical manner to the wild-type albeit on a smaller scale. The removal of the polyhistidine tag from the β-subunit allowed a more straightforward one-step IMAC purification for the point-mutants.

Trypsinolysis of *Mm*α-GluII

*Mm*α-GluII was treated with sequencing grade modified trypsin (Promega) in a 1:100 trypsin: *Mm*α-GluII mass ratio, supplemented with 2 mM $CaCl_2$ for 4 h at room temperature. The trypsinized material was purified on a Superdex 200 column as above.

Differential scanning fluorimetry

Differential scanning fluorimetry (DSF) experiments were set up by mixing the protein of interest in the concentration range of 0.025 - 0.1 mg/ml with SYPRO Orange (Molecular Probes) at a concentration of 5X in a final volume of 50 µl in white, polypropylene, non-skirted PCR plates (Stralab) sealed with optically-clear ThermalSealRT2 film (Alpha

Laboratories). All measurements were done in quadruplicate. A 25 ºC to 80ºC thermal ramp with 1 degree Celsius per minute was performed on a MX3005P real time PCR machine (Stratagene) measuring fluorescence with FAM and ROX filters which correspond approximately to λ_{ex} of 494 nm and λ_{em} of 602 nm.

Enzymology

Glucose detection assay

Cleavage of glucobiose disaccharides (Carbosynth) of different glycosidic linkages was performed by mixing 30 µl of *Mm* α-GluII at 60 nM and 30 µl serially-diluted disaccharide in PCR tubes and incubating at 37 ºC for 30 min. Glucose release was quantified against a 7-point D-glucose standard curve using the Amplex Red Glucose/Glucose Oxidase Assay Kit (Life Technologies) according to the manufacturer's protocol using 50 µl of the previous reaction. Measurements at different pH were carried out as above but 3 µl of 600 nM *Mm* α-GluII was diluted into sodium phosphate buffer of appropriate pH followed by addition of 30 µl of disaccharide at 1 mM final concentration. Measurements were subtracted from disaccharide only containing wells. A Michaelis-Menten model ($V = [S]V_{max}/(K_m+[S])$) was fit to the graph of initial velocity *versus* substrate concentration in order to obtain the values of V_{max}, K_m, and k_{cat}. A substrate inhibition model ($V=V_{max}[S]/(K_m+ [S](1+[S]/K_i))$) was fitted to the nigerose curve.

Continuous α-glucosidase II assay

The rates of 4-methylumbelliferyl α-D-glucopyranoside (4-MUG) (Sigma-Aldrich) hydrolysis by *Mm*α-GluII were measured mixing a 50 µl sample with 50 µl of 4-MUG

and incubating at 37 ºC in 96-well black non-binding surface treated microplates (Corning). Fluorescence was measured continuously for 30 min at λ_{ex} of 355 nm and λ_{em} of 460 nm on a SpectraMax M5 (Molecular Devices) with 40 scans per well, low photomultiplier tube sensitivity and an emission cut-off filter of 455 nm. A *Mm*α-GluII concentration of 20 nM provided the best signal over the course of the assay. 100 mM potassium phosphate buffer at pH 7.2 was used for all dilutions. 4-Methylumbelliferone (4-MU) quantitation was achieved with a five-point standard curve also containing the enzyme. A Michaelis-Menten model ($V = [S]V_{max}/(K_m+[S])$) was fit to the graph of initial velocity *versus* substrate concentration in order to obtain the values of V_{max}, K_m, and k_{cat}.

Purification of oligosaccharide substrates

Free oligosaccharide (FOS) substrates, $Glc_{(1-3)}Man_{(4-7)}GlcNAc_{(1-2)}$ were isolated from cultured cells treated with *N*B-DNJ to prevent endogenous removal of glucoses from the glycans and purified by normal-phase high-performance liquid chromatography (NP-HPLC). These oligosaccharides are liberated from the proteins they were attached to during proteasomal degradation resulting in free glycans in the cell (1). HL60 or CHO cells were cultured to high density (1×10^7 cells/ml) prior to growth in fresh medium containing 1 mM *N*B-DNJ (gifted from Oxford GlycoSciences Ltd.). Following cell culture, the medium was removed and the cells were washed 3 times with PBS by centrifugation. Washed cells were stored at -20 ºC for a short time before thawing and subjected to Dounce homogenization in water. The maximum recovery of FOS was performed using the following conditions. The homogenate from 1-2 x 10^6 cells (0.1-0.2

mg protein) was desalted and deproteinated using solid phase extraction (SPE) by passage through a mixed-bed ion-exchange column (0.2 ml AG50W-X12 (H^+, 100-200 mesh, BioRad) over 0.4 ml AG3-X4 (O^-, 100-200 mesh, BioRad)), pre-equilibrated with water (5 × 1 ml). The homogenate was added to the column which was washed with 4 × 1 ml water, and this eluate containing the FOS was collected. The extracted, purified FOS were then dried by lyophilization.

An alternative method to obtain high mannose $Glc_2Man_9GlcNAc_2$ glycan was through recombinant methods. Transient transfection of HIV gp120 (Bal) in pHLsec was conducted in ExpiCHO (Life Technologies) cells according to the manufacturer's protocol. At the time of transfection, the media was supplemented with 10 μM kifunensine and 200 μM *N*B-DNJ to ensure the *N*-linked glycans on the protein were all high-mannose glycans. The cells were harvested after seven days by centrifugation at 3000 g for 15 min. The protein was purified by immobilized metal affinity chromatography analogously to what described for *Mm*α-GluII above and the eluate was dialyzed into PBS before lyophilization. Glycan ($Glc_3Man_9GlcNAc_2$) was released from the freeze-dried purified recombinant gp120 (kif + *N*B-DNJ treated) with PNGaseF (New England Biolabs) under non-denaturing conditions. Briefly, after resuspending in NEB Glyco Buffer2, PNGaseF was added at 5,000 U/ml and incubated 37°C for 24 hours. The PNGase F digest mix (gp120+glycan) was treated with 60 μL of *Mm*α-GluI at 4 mg/ml at 37 ºC for 48 h, to remove the outer Glc residue off the glycan. Proteins were removed by passing the mix through a MultiScreen-IP Filter Plate, 0.45 μm (Millipore). The free glycan $Glc_2Man_9GlcNAc_2$ was lyophilized before fluorescent 2-AA labeling.

2AA-labeling of oligosaccharide substrates

The free oligosaccharides were labeled with anthranilic acid (2-AA) (Sigma-Aldrich) and purified using Spe-ed amide 2 SPE cartridges (Applied Separations). Anthranilic acid (30 mg/ml) was dissolved in a solution of 4% (w/v) sodium acetate-trihydrate and boric acid (2% w/v) in methanol. This solution was added to solid sodium cyanoborohydride (final concentration 45 mg/ml) (Sigma-Aldrich) and mixed to give the final labeling mixture. A sample of free oligosaccharide (30 µl) was added to 80 µl of labeling mixture and placed at 80 ºC for 45-60 min. The reaction was allowed to cool to room temperature and 1 ml acetonitrile/water (95:5, v/v) added and vortexed.

Purification of 2AA-labeled oligosaccharide substrates

Labeled oligosaccharides were purified by adsorption to Speed-amide SPE columns, washed with acetonitrile/water 95:5 (v/v), and eluted with 2 ml water. Labeled oligosaccharides in 50 mM Tris/HCl buffer, pH 7.2 were further purified using a Concanavalin A (ConA)–Sepharose 4B (Sigma-Aldrich) column (100µl packed resin). The column was pre-equilibrated with 2 × 1 ml water followed by 1 ml of 1 mM $MgCl_2$, 1 mM $CaCl_2$ and 1 mM $MnCl_2$ in water and finally 2 x 1 ml 50 mM Tris/HCl buffer, pH 7.2. An aliquot of 2-AA labeled oligosaccharide was added and allowed to pass through the column before washing with 2 x 1 ml 50 mM Tris/HCl buffer, pH 7.2. The ConA-bound, free oligosaccharides were then eluted with 2 x 1 ml hot (70ºC) 0.5 M methyl α-D-mannopyranoside (Sigma-Alrich) in 50 mM Tris/HCl buffer, pH 7.2. Methyl α-D-

mannopyranoside was removed from ConA-sepharose-purified 2-AA-labeled oligosaccharides in readiness for preparative isolation using porous graphitized carbon (PGC) SPE chromatography. A 1 ml (25 mg) PGC column (Thermo Electron) was pre-equilibrated with 1 ml methanol, followed by 1 ml water, 1 ml acetonitrile containing 0.1% trifluoroacetic acid (TFA) and, finally, 2 x 0.5 ml water. After sample loading the column was washed with 2 x 0.5 ml water before oligosaccharides were eluted with 2 ml 50% acetonitrile containing 0.1% TFA. The final purity of the labeled glycans was greater than 95%.

Cleavage and detection of glycans by normal-phase high-performance liquid chromatography

The 2-AA-labeled glycans were mixed with varying concentrations of *Mm*α-GluII at 37 ºC and incubated for at least 3 h. The reaction was stopped with the addition of 30 µl acetonitrile. Ultrafiltration in a 10 kDa MWCO device (Millipore) was done at 7,000 g for 45 min to separate the glycans from the enzyme. The filtrate was applied to a TSKgel Amide-80 column (Tosoh Bioscience) for NP-HPLC analysis on a Waters Alliance 2695 separations module with an in-line Waters 474 fluorescence detector set at λ_{ex} of 360 nm and λ_{em} of 425 nm. All chromatography was performed at 30 ºC. Solvent A was composed of 20% 100 mM $CH_3CO_2NH_4$, pH 3.85, in Milli-Q water and 80% acetonitrile. Solvent B is composed of 20% 100 mM $CH_3CO_2NH_4$, pH 3.85, in Milli-Q water, 60% Milli-Q water and 20% acetonitrile. A linear gradient from 86% A to 54.7% A over 31.5 min at 0.8 ml/min was used to separate the glycans. Gradient conditions were as follows: time = 0 min (t = 0), 86% solvent A (0.8 ml/min); t = 6, 86% solvent A (0.8 ml/min); t =

35, 54.7% solvent A (0.8 ml/min); t = 37, 5% solvent A (1 ml/min); t = 39, 5% solvent A (0.8 ml/min); t = 41, 86% solvent A (1 ml/min); t = 42, 86% solvent A (1 ml/min); t = 54, 86% solvent A (1.2 ml/min); t = 55, 86% solvent A (0.8 ml/min). Samples were injected in Milli-Q water/acetonitrile (3:7, v/v). Glucose units (GU) were determined, following comparison with a 2-AA-labeled glucose oligomer ladder (derived from a partial hydrolysate of dextran) external standard using Peak Time software (developed in-house). Glucosylated oligosaccharides were identified from the characteristic elution times (GU value) and collected separately.

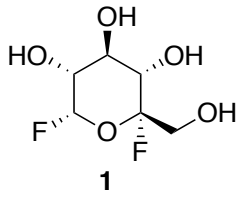

1

5-fluoro-α-D-glucopyranosyl fluoride (1): 2,3,4,6-tetra-*O*-acetyl-5-fluoro-α-D-glucopyranosyl fluoride (126 mg, 342 μmol, 1.0 equiv, prepared from 2,3,4,6-tetra-*O*-acetyl-α-D-glucosyl fluoride as previously described (2, 3)) was cooled to 0 ºC (ice/H_2O bath) and dissolved in NH_3 solution (7 M in MeOH, 8 mL). The ice bath was removed, and the reaction mixture was stirred at room temperature for 3 h. The reaction mixture was concentrated under reduced pressure and purified by flash column chromatography (SiO_2, EtOAc:MeOH = 49:1) to provide **1** (56.5 mg, 282 μmol, 82% yield) as a pale brown oil. NMR characterisation was performed on a Varian Unity Inova 500 instrument, using residual undeuterated solvent as a reference (4). **1:** R_f = 0.18 (SiO_2, EtOAc:MeOH = 49:1); ^{1}H NMR (500 MHz, CD_3OD) (Fig. S9A) δ = 5.66 (dd, J = 56.1, 1.7 Hz, 1 H),

3.93 (dd, J = 17.9, 12.6 Hz, 1 H), 3.84 – 3.72 (m, 3 H), 3.67 (dd, J = 22.5, 12.7 Hz, 1 H) ppm; ^{13}C NMR (125 MHz, CD_3OD) δ = 115.3 (d, J = 220.0 Hz), 107.7 (dd, J = 223.4, 4.7 Hz), 74.3 (d, J = 31.9 Hz), 72.8 (dd, J = 3.9, 1.1 Hz), 71.7 (d, J = 22.5 Hz), 64.1 (d, J = 26.1 Hz).

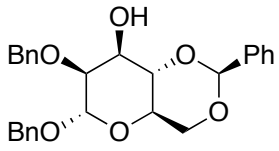

Benzyl 2-*O*-benzyl-4,6-*O*-benzylidene-α-D-mannopyranoside: To a solution of benzyl 4,6-*O*-benzylidene-α-D-mannopyranoside (2.92 g, 8.15 mmol, 1.0 equiv, prepared from D-mannose as previously described (5)) in CH_2Cl_2 (283 mL) were added *n*-Bu_4NHSO_4 (3.04 g, 8.96 mmol, 1.1 equiv) and benzyl bromide (1.06 mL, 8.96 mmol, 1.1 equiv). Finally, aq. NaOH (30% w/v, 23.5 mL) was added. The biphasic mixture was heated to reflux (55 °C, oil bath) and stirred vigorously at the same temperature for 18 h. After cooling to 25 °C, the layers were separated. The organic layer washed with H_2O (100 mL), sat. aq. $NaHCO_3$ (100 mL), and brine (100 mL), dried ($MgSO_4$), filtered and concentrated under reduced pressure. The crude mixture was purified by flash column chromatography (SiO_2, EtOAc:petroleum spirits = 1:9) to provide benzyl 2-*O*-benzyl-4,6-*O*-benzylidene-α-D-mannopyranoside (1.53 g, 3.41 mmol, 42% yield) as a colourless oil. NMR characterisation was performed on a Varian Unity Inova 500 instrument, using residual undeuterated solvent as a reference (4). **Benzyl 2-*O*-benzyl-4,6-*O*-benzylidene-α-D-mannopyranoside:** R_f = 0.19 (SiO_2, EtOAc:petroleum spirits = 4:1); ^{1}H NMR (500 MHz, $CDCl_3$) δ = 7.52 – 7.47 (m, 2 H), 7.42 – 7.28 (m, 13 H), 5.58 (s, 1 H), 4.94 (s, 1 H),

4.73 (d, J = 11.9 Hz, 1 H), 4.71 (AB d, J = 11.9 Hz, 1 H), 4.67 (AB d, J = 11.9 Hz, 1 H), 4.49 (d, J = 11.9 Hz, 1 H), 4.24 (d, J = 5.9 Hz, 1 H), 4.18 – 4.13 (m, 1 H), 3.94 (t, J = 9.2 Hz, 1 H), 3.89 – 3.80 (m, 3 H), 2.35 (d, J = 7.4 Hz, 1 H) ppm; ^{13}C NMR (125 MHz, $CDCl_3$) δ = 137.8, 137.6, 137.2, 129.3, 128.79, 128.76, 128.5, 128.3, 128.21, 128.19, 128.1, 126.5, 102.3, 97.9, 79.8, 78.8, 78.7, 74.0, 69.6, 69.0, 64.0, 60.6 ppm.

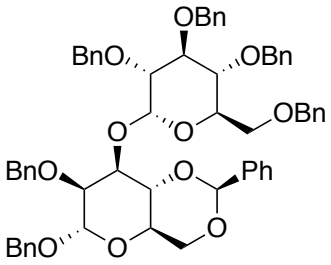

Benzyl *O*-(2,3,4,6-tetra-*O*-benzyl-α-D-glucopyranosyl)-(1→3)-2-*O*-benzyl-4,6-*O*-benzylidene-α-D-mannopyranoside: To a solution of benzyl 2-*O*-benzyl-4,6-*O*-benzylidene-α-D-mannopyranoside (1.53 g, 3.41 mmol, 1.0 equiv) and 2,3,4,6-tetra-*O*-benzyl-α-D-glucopyranosyl trichloroacetimidate (3.04 g, 4.43 mmol, 1.3 equiv) in Et_2O (75 mL) was added freshly activated 3 Å molecular sieves (1.5 g). The mixture was cooled to –30 °C (dry ice/acetone bath) and stirred for 30 min at the same temperature. At the same temperature, trimethylsilyltriflate (620 μL, 3.41 mmol, 1.0 equiv) was added dropwise. The mixture was stirred at the same temperature for 20 hours. The reaction mixture was diluted with EtOAc (300 mL) and filtred through a pad of celite. The filtrate was washed with brine (3 × 100 mL), dried ($MgSO_4$), filtered and concentrated under reduced pressure. The crude mixture was purified by flash column chromatography (SiO_2, EtOAc:petroleum spirits = 1:9) followed by a second flash column chromatography (SiO_2, petroleum spirits:CH_2Cl_2 = 2:8 → 1:9) to provide benzyl *O*-

(2,3,4,6-tetra-*O*-benzyl-α-D-glucopyranosyl)-(1→3)-2-*O*-benzyl-4,6-*O*-benzylidene-α-D-mannopyranoside (1.04 g, 1.08 mmol, 32% yield) as a colourless oil that crystallised on standing. NMR characterisation was performed on a Varian Unity Inova 500 instrument, using residual undeuterated solvent as a reference (4). **1:** R_f = 0.21 (SiO_2, EtOAc:petroleum spirits = 4:1); ^{1}H NMR (500 MHz, $CDCl_3$) δ = 7.44 – 7.41 (m, 2 H), 7.39 – 7.13 (m, 31 H), 7.04 – 7.00 (m, 2 H), 5.56 (d, *J* = 3.5 Hz, 1 H), 5.48 (s, 1 H), 4.98 (d, *J* = 11.0 Hz, 1 H), 4.93 (br s, 1 H), 4.91 (d, *J* = 12.0 Hz, 1 H), 4.86 (d, *J* = 11.0 Hz, 1 H), 4.77 (d, *J* = 8.7 Hz, 1 H), 4.74 (d, *J* = 7.6 Hz, 1 H), 4.71 (d, *J* = 12.9 Hz), 4.58 (d, *J* = 12.3 Hz, 1 H), 4.51 (d, *J* = 12.3 Hz, 1 H), 4.49 – 4.35 (m, 4 H), 4.33 (d, *J* = 12.3 Hz, 1 H), 4.20 (dd, *J* = 9.9, 4.6 Hz, 1 H), 4.01 (t, *J* = 9.2 Hz, 1 H), 3.93 (td, *J* = 10.1, 4.6 Hz, 1 H), 3.89 – 3.80 (m, 3 H), 3.70 – 3.62 (m, 2 H), 3.60 (t, *J* = 9.5 Hz, 1 H), 3.54 (dd, *J* = 9.7, 3.7 Hz, 1 H) ppm; ^{13}C NMR (125 MHz, $CDCl_3$) δ = 138.9, 138.7, 138.4, 138.2, 138.1, 137.6, 137.2, 129.3, 128.59, 128.57, 128.5, 128.44, 128.40, 128.37, 128.35, 128.3, 128.22, 128.19, 128.1, 128.03, 128.00, 127.98, 127.95, 127.92, 127.89, 127.85, 127.8, 127.74, 127.66, 127.63, 127.57, 127.3, 126.6, 102.5, 98.8, 97.1, 81.5, 79.9, 79.2, 77.9, 77.6, 75.6, 75.1, 74.0, 73.5, 73.0, 71.0, 70.8, 69.3, 69.0, 68.7, 64.4 ppm.

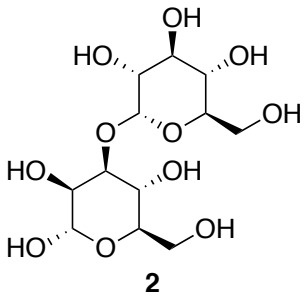

2

α-D-Glucopyranosyl-(1→3)-D-mannopyranose (2): Benzyl *O*-(2,3,4,6-tetra-*O*-benzyl-α-D-glucopyranosyl)-(1→3)-2-*O*-benzyl-4,6-*O*-benzylidene-α-D-mannopyranoside (670 mg, 690 μmol, 1.0 equiv) was dissolved in MeOH (250 mL). Pd/C (10% Pd, 200 mg, 30 weight-%) and $Pd(OH)_2$/C (10% $Pd(OH)_2$, 200 mg, 30 weight-%) were added. The mixture was stirred under an atmosphere of H_2 for 16 h. The reaction mixture was filtered through celite and concentrated under reduced pressure to provide **2** (212 mg, 619 μmol, 90% yield) as an approx. 2:1 mixture of anomers as a clear, colourless oil. NMR characterisation was performed on a Varian Unity Inova 500 instrument, using residual undeuterated solvent as a reference (4). **2:** ^{1}H NMR (500 MHz, D_2O) (Fig. S9B) δ = 5.34 – 5.30 (m, 1 H), 5.23 (s, 0.63 H), 4.99 (s, 0.37 H), 4.18 – 4.15 (m, 1 H), 4.05 – 3.98 (m, 1 H), 3.97 – 3.79 (m, 8 H), 3.64 (dd, *J* = 10.0, 3.7 Hz, 1 H), 3.52 – 3.46 (m, 1 H) ppm; ^{13}C NMR of major anomer (125 MHz, D_2O) δ = 101.2, 94.6, 78.9, 73.5, 73.1, 73.0, 72.4, 71.2, 70.2, 66.8, 61.5, 61.2 ppm. ^{13}C NMR of minor anomer (125 MHz, D_2O) δ = 101.0, 94.2, 82.4, 81.5, 76.6, 73.5, 72.4, 71.8, 70.3, 66.6, 61.6, 61.2 ppm.

X-ray crystal structures determination

Crystal growth

All crystallization solutions were purchased from Molecular Dimensions. Filtered *Mm*α-$GluII_{Tryps}$ at 5.6 mg/ml was crystallized by vapor diffusion with 21% v/v ethylene glycol, 11% w/v PEG 8000 (from the Morpheus Precipitant Mix 2), 50 mM Morpheus carboxylic acids mix, 100 mM Morpheus buffer system 1 pH 6.25 (all solutions from Molecular Dimensions) in a 3:1 protein:precipitant ratio. 200 μm long rods formed after about one week at 18 ºC. Crystals were transferred into a solution of 16% w/v PEG 8000,

50 mM Morpheus carboxylic acids mix, and 100 mM Morpheus buffer system 2 pH 7.2, 20% v/v PEG 400 with or without ligands before cooling in liquid nitrogen. All ligands were sourced from Sigma with the exception of 5-fluoro-α-D-glucopyranosyl fluoride (see above synthesis), *N*B-DNJ (gifted from Oxford GlycoSciences Ltd.), and M*O*N-DNJ, which was synthesized and spectroscopically identical to previous reports. (European Patent Office Publication WO2010096764 (A1)). The D-glucal soak was performed by transferring a crystal to the mother liquor with 15% w/v D-glucal dissolved beforehand. The remaining soaks were performed at the following concentrations: 10 mM glucose, 20 mM 5-fluoro-α-D-glucopyranosyl fluoride, 10 mM castanospermine, 50 mM DNJ, 10 mM *N*B-DNJ and 10 mM M*O*N-DNJ. Iminosugar soaks were performed overnight whereas all others were cryo-cooled within 15 minutes.

X-ray diffraction

Diffraction from *Mm*α-GluII$_{Tryps}$ crystals was measured at the Diamond Light Source (DLS), Harwell, England, UK, except for the apo and *N*B-DNJ structures, data for which were collected respectively on beamlines ID30-1 and BM14 at the ESRF, Grenoble, France. All experiments were carried out at T = 90 K in a stream of cryogenic N_2 gas. Beamlines and wavelengths: Apo: ID30-1@ESRF, λ = 0.96597 Å; Glucal soak: I02@DLS, λ = 0.97910 Å; 5F-Glucosyl fluoride soak: I03@DLS, λ = 1.07227 Å; Glucose soak: I04@DLS, λ = 0.97949 Å; castanospermine and DNJ: I04@DLS, λ = 0.97950 Å; *N*B-DNJ: BM14@ESRF, λ = 0.97880 Å; M*O*N-DNJ: I02@DLS, λ = 1.0721 Å.

Data processing, structure determination and refinement

X-ray diffraction images were processed using the autoPROC (6) or the xia2 (7) suite of programs, which index and integrate with XDS (8), and were scaled and merged using the CCP4 (9) suite of programs, Pointless, Aimless and Truncate. Molecular replacement leading to structure determination of the apo form was performed with Phaser (10) also part of the CCP4 suite, run with the automated MR pipeline MrBUMP (11), using chain A of the PDB entry 3L4Z as a search model. Model building was performed with Coot and Buccaneer (12, 13), and refinement with autoBUSTER, using LSSR restraints (14, 15). Model validation was carried out with internal modules of Coot and through the MolProbity server (16). Initial sets of phases for the 5F-glucosyl fluoride, glucal, glucose and iminosugar soaks were obtained by molecular replacement from the apo structure. Idealized coordinates and stereochemical dictionaries for ligands not present in the autoBUSTER libraries and non-standard ligands were generated using the GRADE server starting from SMILES strings (http://grade.globalphasing.org/). Each ligand was docked in the unbiased Fo-Fc difference electron density map calculated from the phases at the end of the iterative protein-only model building and refinement, and the GRADE-generated stereochemical dictionary was used in Coot to fit the ligand to the difference map, varying its conformations around its torsional degrees of freedom. A final round of refinement of the protein and docked ligand utilized ligand stereochemical restraints from the GRADE-generated dictionary. All figures were produced in PyMOL.

Hydrogen-deuterium exchange mass spectrometry

HDX experiments were performed using a Waters HDX Manager and Acquity UPLC M-Class system coupled to a Synapt G2Si instrument (Waters). The UPLC system consisted

of an in-line pepsin column (Enzymate BEH 5µm, 2.1 x 30mm, Waters), C18 trap column (Acquity UPLC BEH C18 1.7µm VanGaurd, Waters) and C18 analytical column (Acquity UPLC BEH C18 1.7µm, 1 x 100 mm, Waters). Samples were diluted to 10µM in 50mM HEPES, 150mM NaCl pH7 and kept at 1 ºC until D_2O labeling. Labeling was done at 20 ºC from 15 s to 60 min (15 s, 30 s, 1 min, 5 min, 10 min, 30 min, 60 min time points). The labeling solution was 50 mM HEPES, 150 mM NaCl in 99.99% D_2O pH 6.6 and samples were quenched with a 50 mM HEPES, 150 mM NaCl pH 1.2 solution. Samples were digested for 2 min at 20 ºC and desalted on the trap column at a flow rate of 40 µl/min (95% buffer A; 0.1% formic acid in water and 5% buffer B; 0.1% formic acid in acetonitrile) at 0 ºC. Digested peptides were eluted over the analytical column to the mass spectrometer over a 10 min gradient (5% to 35% buffer B) at 40 µl/min. The mass spectrometer was set for positive ions detection in Tof mode. Data was acquired with MassLynx 4.1 software and analyzed with ProteinLynx Global Server and DynamX software (Waters).

At*α-GluII *in planta

RNA isolation and cloning of fluorescent constructs

Total RNA was isolated from *A. thaliana* Col-0 leaves using the Plant RNA purification reagent (Invitrogen) and cDNA synthesis was performed using Super script III First-Strand Synthesis System (Invitrogen). The full-length coding sequence of *At*GluIIα and *At*GluIIβ were amplified by PCR using the Accuprime Pfx DNA Polymerase (Invitrogen), cloned into pENTR-D Topo vector (Invitrogen) and sequenced. *At*GluIIα mutants were generated by fusion of two separate PCR products via overlapping

primers as described in (17), cloned into pENTR-D Topo vector and sequenced. DNA primers for cloning and mutagenesis:

*At*GluIIα F: caccATGAGATCTCTTCTCTTTGTAC;

*At*GluIIα R: CAGAATCTTTACGGTCCAG;

*At*GluIIβ F: caccATGAGAGTAGTAGTAATATCTTC;

*At*GluIIβ R: TCAGAGTTCGTCGTGATTCTGAGG;

*At*GluIIα^{R787E} F: GGAAGGACCGGTTTAGGgaAAGTTCCTCTCAAATGGAC;

*At*GluIIα^{R787E} R: GTCCATTTGAGAGGAACTTtcCCTAAACCGGTCCTTCC;

*At*GluIIα$^{R787E/R784E}$ F: CCAAGGAAGGACgaGTTTAGGgaAAGTTCCTCTCAAATG;

*At*GluIIα$^{R787E/R784E}$ R: CATTTGAGAGGAACTTtcCCTAAACtcGTCCTTCCTTGG.

*At*GluIIα wild-type and mutants were fused at the C-terminal with the enhanced GFP (eGFP), using the pK7FWG2 binary vector. The *At*GluIIα double mutant was also fused at the C-terminal with the monomeric RFP (mRFP) into the pB7RWG2 binary vector whereas *At*GluIIβ was fused at the N-terminal with mRFP using the pH7WGR binary vector, using LR Gateway technology (Invitrogen). Binary vectors, containing each construct, were cloned and then amplified in *Escherichia coli* DH5α before transformation in *Agrobacterium tumefaciens* (strain GV3101).

Plant materials and growth conditions

Transient transformation of 4-5 weeks old tobacco leaf epidermal cells (*Nicotiana tabacum* plants, cv Petit Havana) was performed. Plants were grown at 25 ºC, 14 h light, 10 h dark and were used for *Agrobacterium tumefaciens* (strain GV3101)-mediated

transient expression (18, 19). The bacterial optical density (OD_{600}) used for plant transformation was 0.5 for all constructs.

Confocal laser scanning microscopy

An inverted laser scanning confocal microscope (LSM Pascal; Carl Zeiss) was used for confocal analyses. Imaging of *At*GluIIα-GFP and *At*GluIIα-GFP single mutants were performed using 488 nm excitation of an Argon ion laser, 25 mW. Imaging of *At*GluIIα-RFP double mutant and *At*GluIIβ-RFP were performed using a 543 nm excitation He/Ne laser, 50mW. GFP was detected with a 505–530 nm filter set whereas RFP was detected with a 560–615 nm filter set. A 488/543/633 beam splitter was used for acquisition. Imaging was performed using 40x Zeiss plan-neofluar oil, 1.3 NA, DIC.

Protein extraction and (co-)immunoprecipitation

Agrobacterium-infiltrated tobacco leaves were used to prepare total protein extracts. Total extracts were prepared as previously described (20). Adult leaves (approximately 1 g) from 4-week-old plants were frozen in liquid nitrogen, homogenized with mixer mill MM301 (Retsch) for 1 min at 30 Hz and taken up in cold extraction buffer [50 mM Tris-HCl pH 8, 150 mM NaCl, 10% glycerol, 1% w/v Nonidet P-40, 10 mM EDTA, 1 mM PMSF protease inhibitor mixture (Sigma)]. After incubation for 2 h at 4 ºC with gentle shaking, this preparation was filtered through Miracloth and centrifuged at 18,000 g for 30 min. The supernatant was incubated overnight at 4 ºC with RFP-Trap_MA or GFP-Trap_MA (Chromotek) used for controls. The beads were collected, washed three times with ice-cold extraction buffer and once with 50 mM Tris-HCl pH 7.5. Proteins that were

retained on the beads were separated by SDS–PAGE 7% w/v and analyzed by western blot with anti-RFP or GFP monoclonal antibodies (Chromotek).

Small angle X-ray scattering (SAXS) of *Mm*α-GluII and *Mm*α-GluII$_{Tryps}$

SAXS data for *Mm*α-GluII and *Mm*α-GluII$_{Tryps}$ were collected at the BM29 beamline at the European Synchrotron Radiation Facility, Grenoble, France. The wavelength was set at 0.992 Å and transmission was at 100%, with images recorded on a Pilatus 1M detector set to a distance of 2.886 m. Calibration was conducted with measurements on albumin or glucose oxidase in order to derive molecular weights from I_0 values. All measurements were carried out in 150 mM NaCl and 20 mM HEPES at pH 7.4. A twofold dilution series with six concentrations between 4.12 mg/ml and 0.13 mg/ml was measured for *Mm*α-GluII$_{Tryps}$ and a twofold dilution series with five concentrations between 2.97 mg/ml and 0.17mg/ml was measured for *Mm* α-GluII. 30 µl of each sample were flowed through a quartz capillary taking 10 x 1 s images. Automated image processing followed by buffer subtraction as part of the processing pipeline at the beamline allowed scattering curves to be used for further data processing. SAXS data were processed using the ATSAS (21) software suite. Using PRIMUS (22), for both *Mm*α-GluII and *Mm*α-GluII$_{Tryps}$ samples, the low-angle region of the low concentration scattering curves were merged with the high angle regions of the high-concentration profile. This was done to compensate for interparticle effects at high concentration. The radius of gyration was determined using PRIMUS (22), and D_{max} was calculated from the pair distribution function calculated by GNOM (23). Ten bead models were created for each structure by DAMMIN (24) and then aligned and averaged using DAMAVER (25). DAMMIN was

then used to compare the averaged model against raw data using reduced χ^2 values. All models possess $0.9<\chi^2<1.1$ against raw data. The crystal structure of *Mm*α-GluII$_{Tryps}$ crystal structure was initially fitted to the *Mm*α-GluII$_{Tryps}$ SAXS envelope using SUPCOMB(26). Chimera (27) was used to convert the SAXS envelopes to maps (command MOLMAP, using a 2.5 nm filter) and superpose the *Mm*α-GluII SAXS map to the *Mm*α-GluII$_{Tryps}$ SAXS map and model.

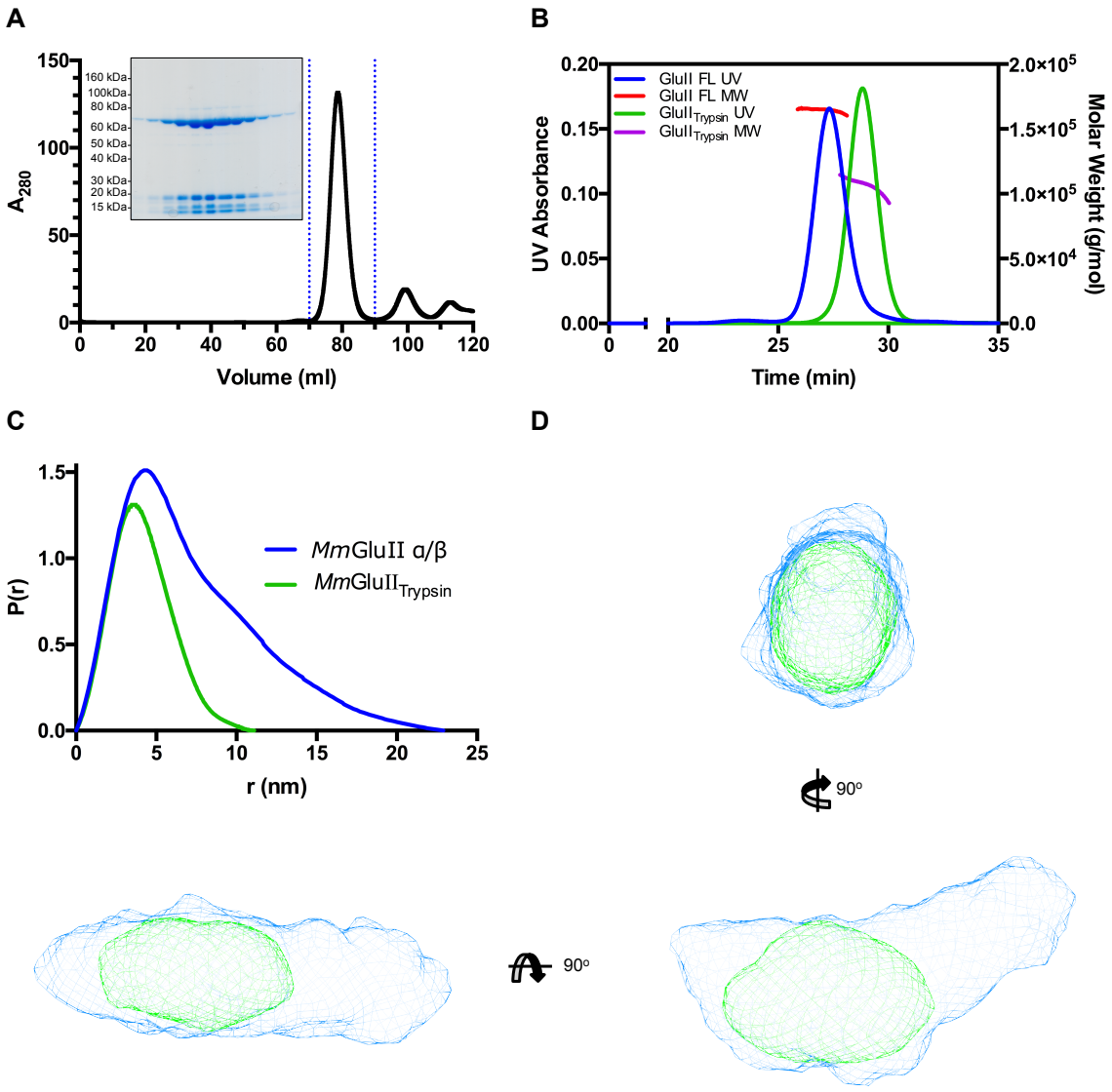

Figure S1. Biochemical and structural characterization of the *Mm*α-GluII$_{Tryps}$ fragment. (**A**) Gel filtration purification of the *Mm*α-GluII$_{Tryps}$ fragment. Chromatogram after 4 h incubation of *Mm*α-GluII with trypsin on a Superdex 200 16/600 column. Inset: SDS-PAGE analysis of the fractions indicated within the blue lines. (**B**) Size-exclusion chromatography multi-angle laser light scattering (SEC-MALLS) of *Mm*α-GluII. and *Mm*α-GluII$_{Tryps}$. Samples were separated on a Superdex 200 10/300 (GE Life sciences) column pre-equilibrated in PBS. Samples were analyzed using a Prominence HPLC (Shimadzu) at 0.5 ml/min with an online UV, refractive index and a Dawn HELEOS 8+

441 (Wyatt Technologies) multi-angle laser light scattering detector set to 662.3 nm. Peaks
442 were analyzed with a Zimm model using a refractive index increment of 0.185 ml/g. (**C**)
443 P(r) functions from analysis of SAXS data. D_{max} was calculated from the pair distribution
444 function calculated by GNOM (23). (**D**) Three orthogonal views of the SAXS hydrated
445 envelopes for *Mm* α-$GluII_{Tryps}$ (green mesh) and wt *Mm* α-GluII (light blue mesh),
446 overlayed in Chimera (27).
447

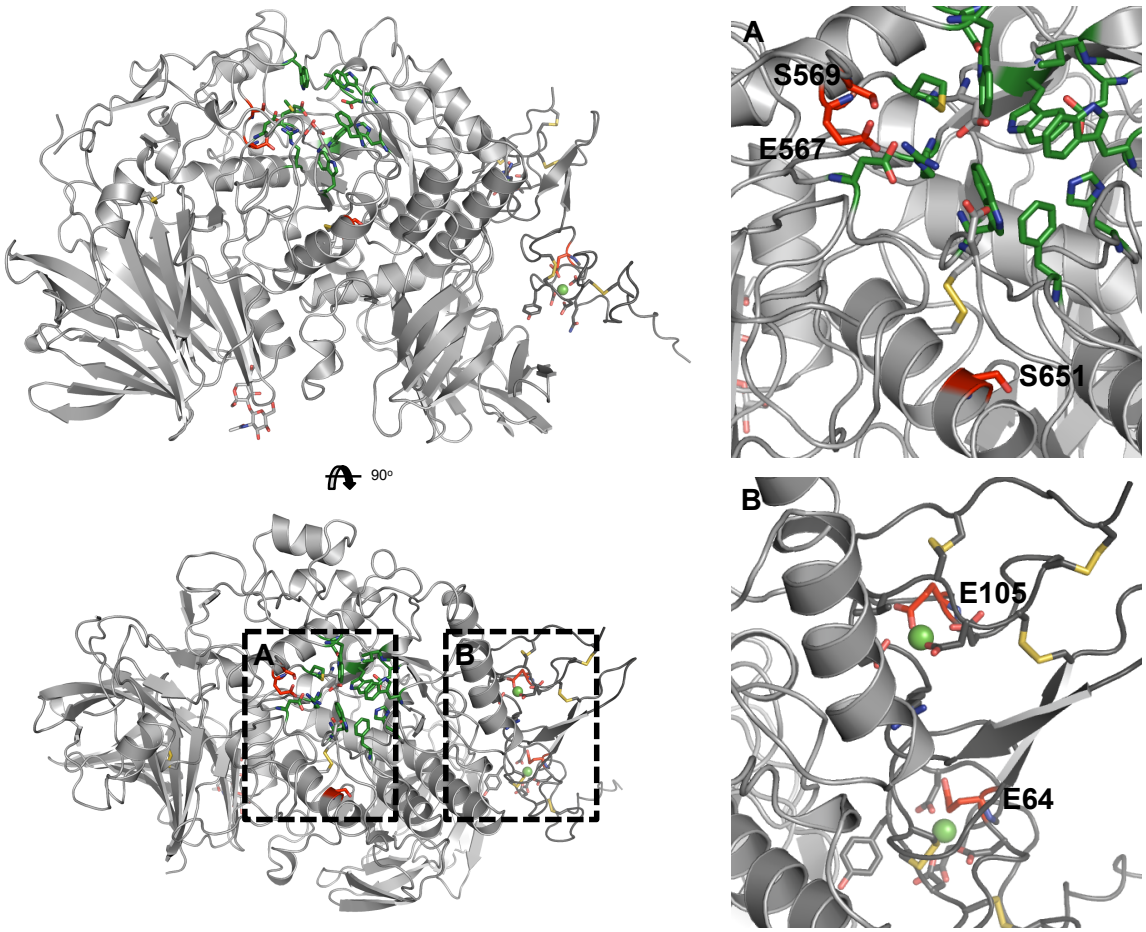

Figure S2. Mapping of inactive mutants onto the *Mm*α-GluII$_{Tryps}$ structure. (**A**) The *Mm*α-GluII α-subunit inactive E567Q mutant (28) and the *Arabidopsis thaliana* psl5-1 inactive mutant (*At*α-GluII α-subunit S517F) (29) corresponding to *Mm*α-GluII α-subunit S569F, are in proximity of the active site (in green stick representation). The *Arabidopsis thaliana* rsw3 inactive mutant (*At*α-GluII α-subunit S599F) corresponding to *Mm*α-GluII α-subunit S651F, destabilizes the core of the α-subunit. (**B**) The *S. pombe* α-GluII β-subunit E73A and E114A inactive mutants (30), corresponding to *Mm*α-GluII β-subunit E64A and E105A, disrupt the fold on the β-subunit because these glutamic acid residues are needed to coordinate the Ca^{2+} ions in the LDLRa β-subunit subdomains.

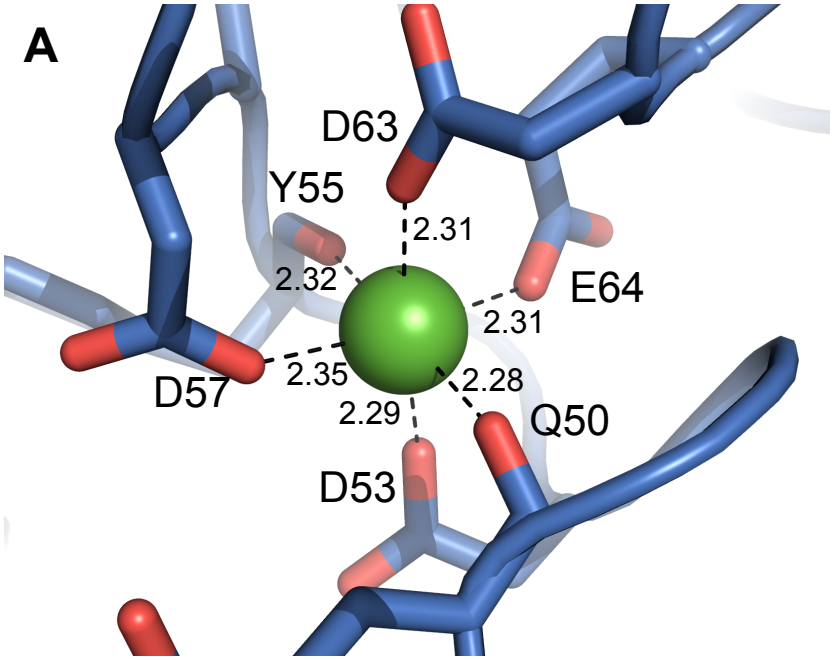

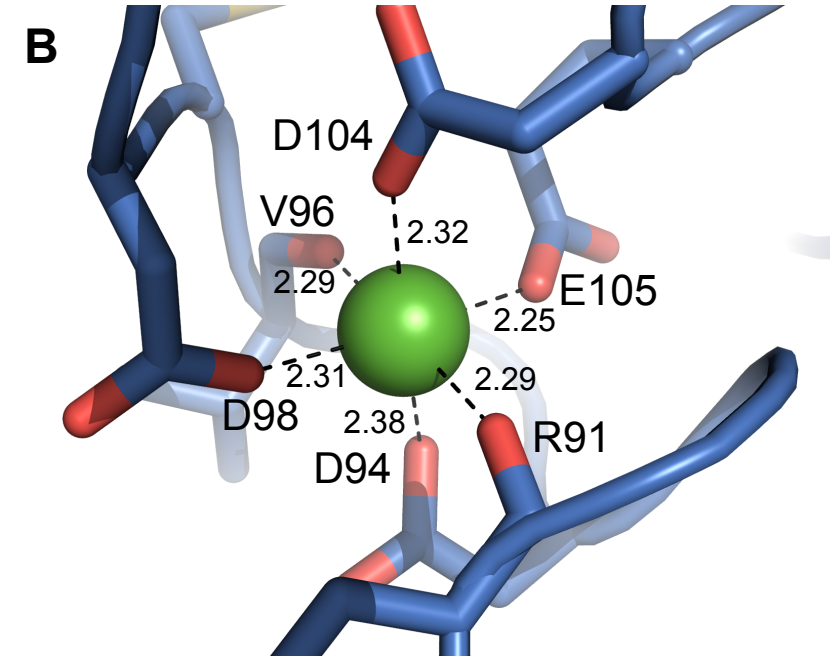

C

```
HsPRKCSH    30  FYDE..SKPFTCLDGSATIPFDQVNDDYCDCKDGSDEPGTAACPN
MmPRKCSH    30  FYEE..SKPFTCLDGTATIPFDQVNDDYCDCKDGSDEPGTAACPN
AtPRKCSH    47  YYKS..SSEIKCKDGSKKFTKAQLNDDFCDCSDGTDEPGTSACPT
SpPRKCSH    37  LYKPDAKGNWKCLGSDKLISFNQVNDDYCDCPDGSDEPGTSACHN

HsPRKCSH    73  GSFHCTNTGYKPLYIPSNRVNDGVCDCCDGTDEYNSGVICENTCK
MmPRKCSH    73  GSFHCTNTGYKPLYILSSRVNDGVCDCCDGTDEYNSGTVCENTCR
AtPRKCSH    90  GKFYCRNAGHSPVILFSSRVNDGICDCCDGSDEYDGHVSCQNTCW
SpPRKCSH    82  GKFFCKNTGYISSYIPSNRVDDTVCDCCDGSDE..SLIKCPNTCA
```

Figure S3. The calcium ions in the N-terminal LDLRa subdomains of the *Mm*α-GluII β-subunit. (**A**) First Ca^{2+} ion, (**B**) second Ca^{2+} ion. Distances from coordinating atoms are indicated in Å. Blue: Carbon. Red: Oxygen. Green: Calcium. H atoms omitted. The dimensionless CBVS(31) values computed from the geometry of the octahedral coordination sphere were 2.38 and 2.41 for the first and the second calcium ion, respectively, and confirm their chemical identity: $CBVS = S_j \exp((d_{Ca0} - d_{ij})/b)p_j$, where d_{Ca0} is the Calcium bond valence radius 1.967 Å, d_{ij} is measured from the model, b is a 'universal constant' of 0.37 Å, and p_j is the occupancy of the ligand, which in this case is always 1.0. CBVS values for a few commonly occurring metal ions: Ca^{2+}: 2.0. Mg: 4.19. Fe^{3+}: 5.26 Fe^{2+}: 3.75; Zn^{2+}: 4.07; Mn^{2+}: 3.23 (from (31)). The structure explains the known *S. pombe* β-subunit mutants E73A and E114A, inactive against Glc_1Man_9(30): both residues are part of a calcium ion coordination sphere in one of the β-subunit LDLRa subdomains (β E64 and E105 in *Mm*α-GluII). (C) Sequence alignments of selected stretches of sequence in the α-Glu II β-subunit in four eukaryotes: *Hs*: *Homo sapiens*; *Mm*: *Mus musculus*; *At*: *Arabidopsis thaliana*; *Sp*: *Schizosaccharomyces pombe*. Magenta squares indicate the Ca^{2+}-binding residues, respectively. Blue triangles show the residues involved in the interface with the α-subunit.

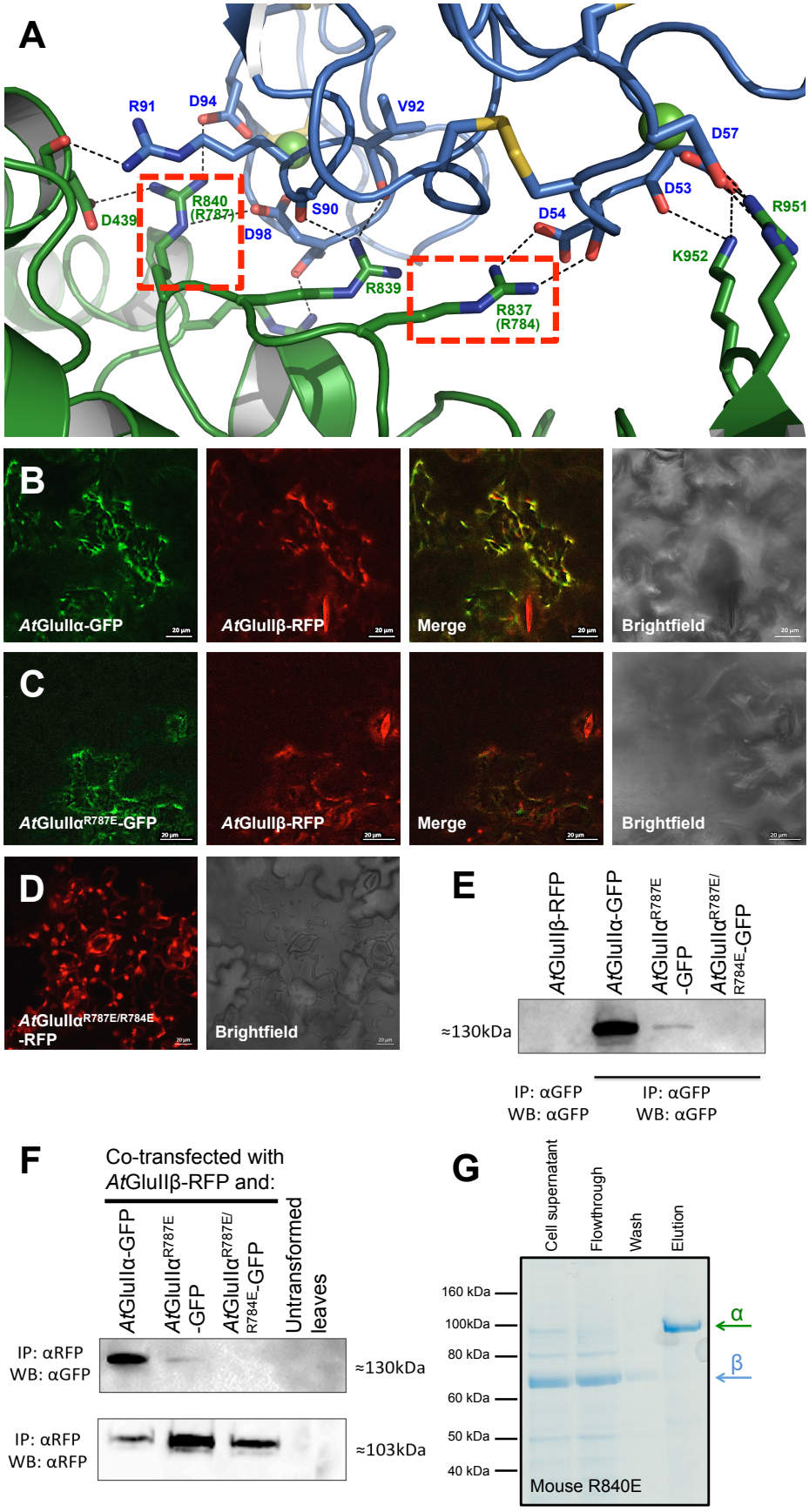
A
R91
D94
V92
D57
D53
R951
R840
(R787)
D439
S90
D98
D54
K952
R839
R837
(R784)
B
AtGlulIα-GFP
AtGlulIβ-RFP
Merge
Brightfield
C
AtGlulIαR787E-GFP
AtGlulIβ-RFP
Merge
Brightfield
D
AtGlulIαR787E/R784E
-RFP
Brightfield
E
AtGlulIβ-RFP
AtGlulIα-GFP
AtGlulIαR787E
-GFP
AtGlulIαR787E/
R784E-GFP
≈130kDa
IP: αGFP
WB: αGFP
IP: αGFP
WB: αGFP
F
Co-transfected with
AtGlulIβ-RFP and:
AtGlulIα-GFP
AtGlulIαR787E
-GFP
AtGlulIαR787E/
R784E-GFP
Untransformed
leaves
IP: αRFP
WB: αGFP
≈130kDa
IP: αRFP
WB: αRFP
≈103kDa
G
Cell supernatant
Flowthrough
Wash
Elution
160 kDa
100kDa
80 kDa
60 kDa
50 kDa
40 kDa
α
β
Mouse R840E

Figure S4. The N-terminal domain of the β-subunit of α-GluII mediates its contact to the α-subunit. (**A**) Details of the Mmα-GluII$_{Tryps}$ α/β interface in the crystal. Carbon atoms in the α- and β-subunits are green and blue, respectively. Red: oxygen; dark blue: nitrogen; yellow: sulfur. The two calcium ions in the β-subunit are depicted as green spheres. H atoms omitted. Highlighted in dashed red rectangles are the two conserved Arg residues that were mutated to validate the interface *in vitro* and *in planta* (the numbers in parentheses refer to the *Arabidopsis thaliana* sequence). (**B,C,D**) *At*GluIIα-GFP, *At*GluIIα^{R787E}-GFP and *At*GluIIα$^{R784E-R787E}$-RFP fusion proteins. Confocal optical sections of *Nicotiana tabacum.* (**B**) Transient expression of *At*GluIIα-GFP and *At*GluIIβ-RFP. The two subunits co-localize in the ER. (**C**) Transient expression of *At*GluIIα^{R787E}-GFP and *At*GluIIβ-RFP. The two subunits still co-localize in the ER. (**D**) Fluorescence microscopy of tobacco leaves transfected with the *At*α-GluII α-subunit double mutant R784E/R787E, initially fused with GFP, did not show any fluorescence. Since GFP fluorescence is reported to be quenched in acidic subcellular compartments (32), to test the hypothesis that the doubly mutated *At*α-GluII α-subunit loses ER localization and is routed to an acidic compartment, *e.g.* lytic vacuoles or autophagosomes, we fused the *At*α-GluII α-subunit R784E/R787E double mutant with RFP (whose fluorescence is pH-independent) instead. Transient expression of *At*GluIIα$^{R784E/R787E}$-RFP fusion protein gives fluorescence that doesn't highlight the ER network. It is localized in a different compartment, probably corresponding to autophagosomes or lytic vacuoles. Scale bar = 20 μm. (**E**) Immunoprecipitation using anti-GFP (α-GFP) and western blotting of tobacco leaves extracts (α-GFP). Leaves were transfected with *At*GluIIβ-RFP, *At*GluIIα-GFP, *At*GluIIα-GFP single mutant R787E, *At*GluIIα-GFP double mutant R784E/R787E and

503 detected with α-GFP antibodies. (**F**) Co-immunoprecipitation using anti-RFP (α-RFP)
504 and western blotting of tobacco leaves extracts using α-GFP and/or α-RFP antibodies.
505 Leaves were co-transfected with *At*GluIIβ-RFP and *At*GluIIα-GFP, *At*GluIIα-GFP single
506 mutant R787E, *At*GluIIα-GFP double mutant R784E/R787E and detected with α-GFP
507 antibodies (top panel) or with α-RFP antibodies (bottom panel). (**G**) SDS-PAGE analysis
508 of the IMAC purification of *Mm*α-GluII point mutant R840E. The β-subunit cannot
509 associate with the His-tagged mutant α-subunit**,** and flows straight through the Nickel
510 column.
511

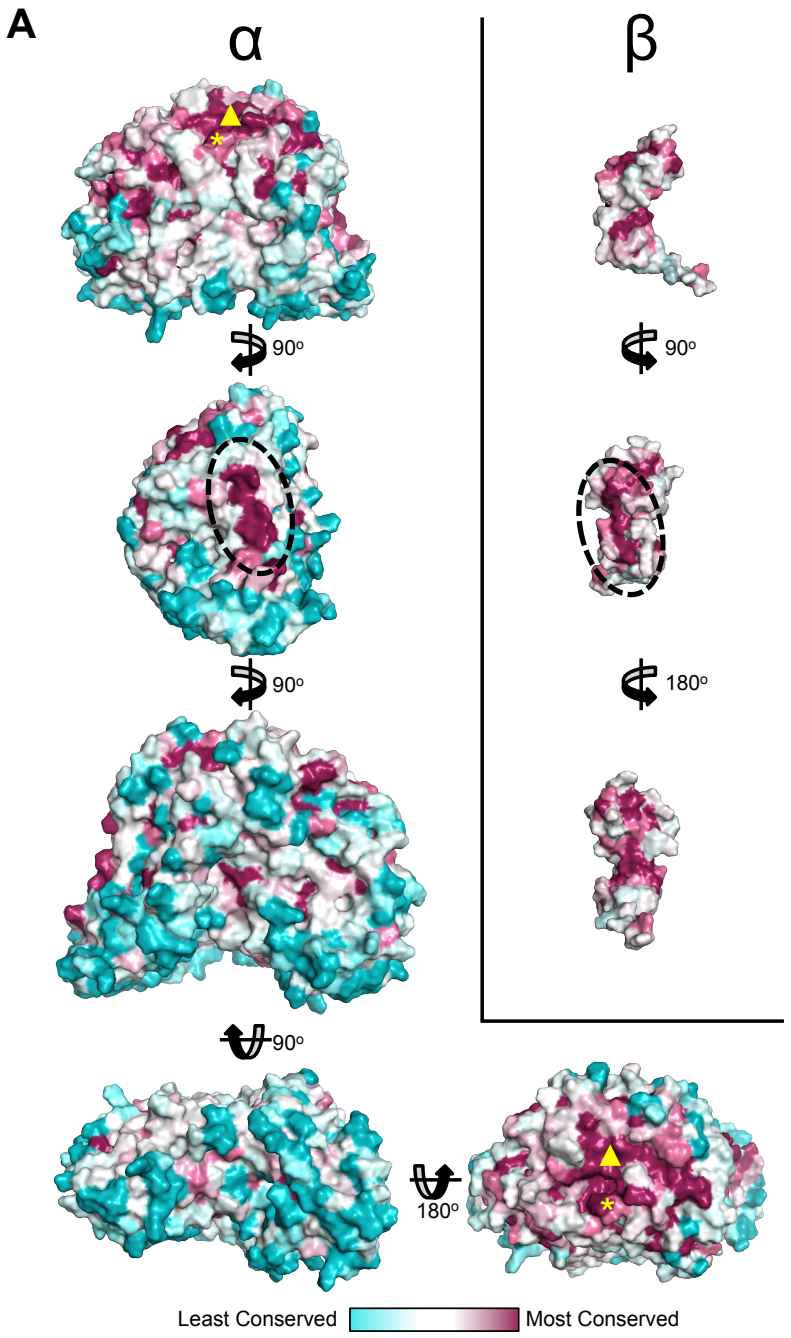

B

```
HsGANAB          556  APNLFVWNDMNEPSVFNGPEVT
MmGANAB          556  APNLYVWNDMNEPSVFNGPEVT
AtGANAB(psl5)    504  TPSLYTWNDMNEPSVFNGPEVT
SpGANAB(gls2)    516  DKNLWIWNDMNEPSVFRGPETS

HsGANAB          630  SQRFGAVWTGDNTAEWEHLKISI
MmGANAB          630  SQRFGAVWTGDNTAEWEHLKISI
AtGANAB(psl5)    578  TQRYGAAWTGDNTAEWEHLRVSI
SpGANAB(gls2)    590  TSALAANWIGDTMTTWEHLRGSI

HsGANAB          830  TLVPRWMRVRRSSECM
MmGANAB          830  TLVPRWMRVRRSSDCM
AtGANAB(psl5)    777  TLIPRKDRFRRSSSQM
SpGANAB(gls2)    790  NLLITREKIRRAAELT
```

C

```
MmGANAB          302  YNLDVFQYELN
HsCtMGAM         1154 FSRDQ..PPGY
HsCtSI           1134 FTRDQ..PPGY
HsNtMGAM         286  FNRDI..TPNG
HsNtSI           261  FTRDQ..LPGD

MmGANAB          556  APNLYVWNDMNEPSVFNGPEVT
HsCtMGAM         1412 LKFDGMWFDMNEPSSFVNGAVS
HsCtSI           1386 MKFDGLWFDMNEPSSFVNGTTT
HsNtMGAM         521  VEFDGIWFDMNEVSNFVDGSV.
HsNtSI           497  VQYDGLWFDMNEVSSFIQGST.

MmGANAB          630  SQRFGAVWTGDNTAEWDHLKISI
HsCtMGAM         1516 SGRWAGHWLGDNTAAWDQLKKSI
HsCtSI           1490 SGRWGGHWLGDNYAAWDNMDKSI
HsNtMGAM         618  SGKFAAHWLGDNTATWDDLRWSI
HsNtSI           594  SGRHAAHWLGDNTASWEQMEWSI
```

Figure S5. (A) Sequence conservation painted on the surface of the *Mm*α-GluII$_{Tryps}$ crystal structure. The dashed line marks the footprint of each subunit onto the other. A yellow asterisk marks the location of the conserved exclusion loop. Residue F307 is part of a conserved ring of aromatic residues (marked by a yellow triangle) between the α-Glu II +1 and +2 subsites, comprising F307, W423, F674 and H700. The figure was obtained by plotting conservation across an alignment of 29 eukaryotic α-GluII sequences using the program Consurf (33). **(B)** Sequence alignments of selected stretches of sequence in the α-Glu II α-subunit in four eukaryotes: *Hs*: *Homo sapiens*; *Mm*: *Mus musculus*; *At*: *Arabidopsis thaliana*; *Sp*: *Schizosaccharomyces pombe*. Magenta and orange squares indicate the nucleophilic and acid/base catalytic Asp residues, respectively. Green triangles show the conserved Arg residues in the interface with the β-subunit. **(C)** Sequence alignments of selected stretches of sequence in the α-Glu II α –subunit with the corresponding ones in human intestinal α-glucosidases. Ct(Nt)MGAM: C-terminal (N-terminal) domain of maltase-glucoamylase; Ct(Nt) SI: C-terminal (N-terminal) domain of sucrase-isomaltase. Blue boxes: exclusion loop insertion. Magenta and orange squares: see **(B)** All alignments were produced in ESPript using the server at ESPript - http://espript.ibcp.fr (34).

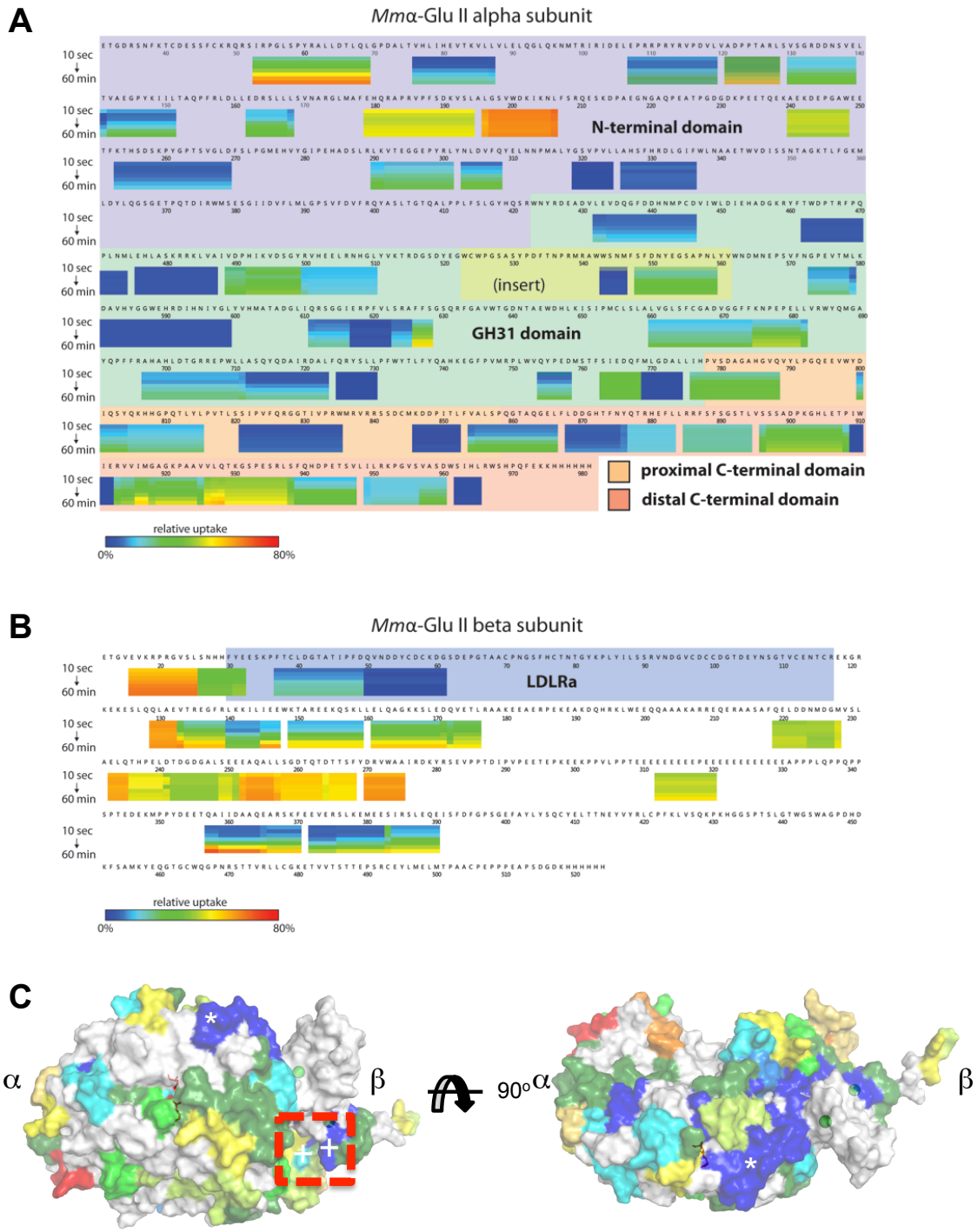

Figure S6. Hydrogen deuterium exchange mass spectrometry of wt *Mmα*-GluII.

Following pepsinolysis, a total of 158 peptides were detected (101 from the α-subunit and 57 from β-subunit) that support the observed α/β interface. Peptides including residues α 837-840 and β 94-98 were not detected, however good coverage was observed for

residues α 951-952 and β 50-61, which were protected from deuterium uptake for up to 60 minutes (Figs 5A,B), consistent with the α/β interface in the crystals. (**A,B**) Heat maps of full-length wt *Mm*α-GluII α- and β-subunits, with the extent of H/D exchange from 10 seconds to 60 minute time points. The α-subunit N-terminal (purple), GH31 (green) +insert (yellow) and C-terminal proximal (orange) and distal (red) domains are highlighted. The β-subunit LDLRa subdomains present in the crystal structure of *Mm*α-GluII$_{Tryps}$ are highlighted in blue. (**C**) Surface representation of *Mm*α-GluII$_{Tryps}$ coloured by rate of Hydrogen-Deuterium Exchange obtained from the wt *Mm*α-GluII. From red (high exchange) to blue (no exchange) through orange, yellow and green: white: no data available. The catalytic residues D564 and D640 are in red sticks. The Calcium ions in the β-subunit are green spheres. The α/β interface residues α -951-952 and β -50-61, protected from H/D exchange, are boxed by a dashed red line and marked by white "+" signs. The helices α 427-441 and α 470-482, protected by the β-subunit in the context of the wt heterodimer are marked by a white asterisk.

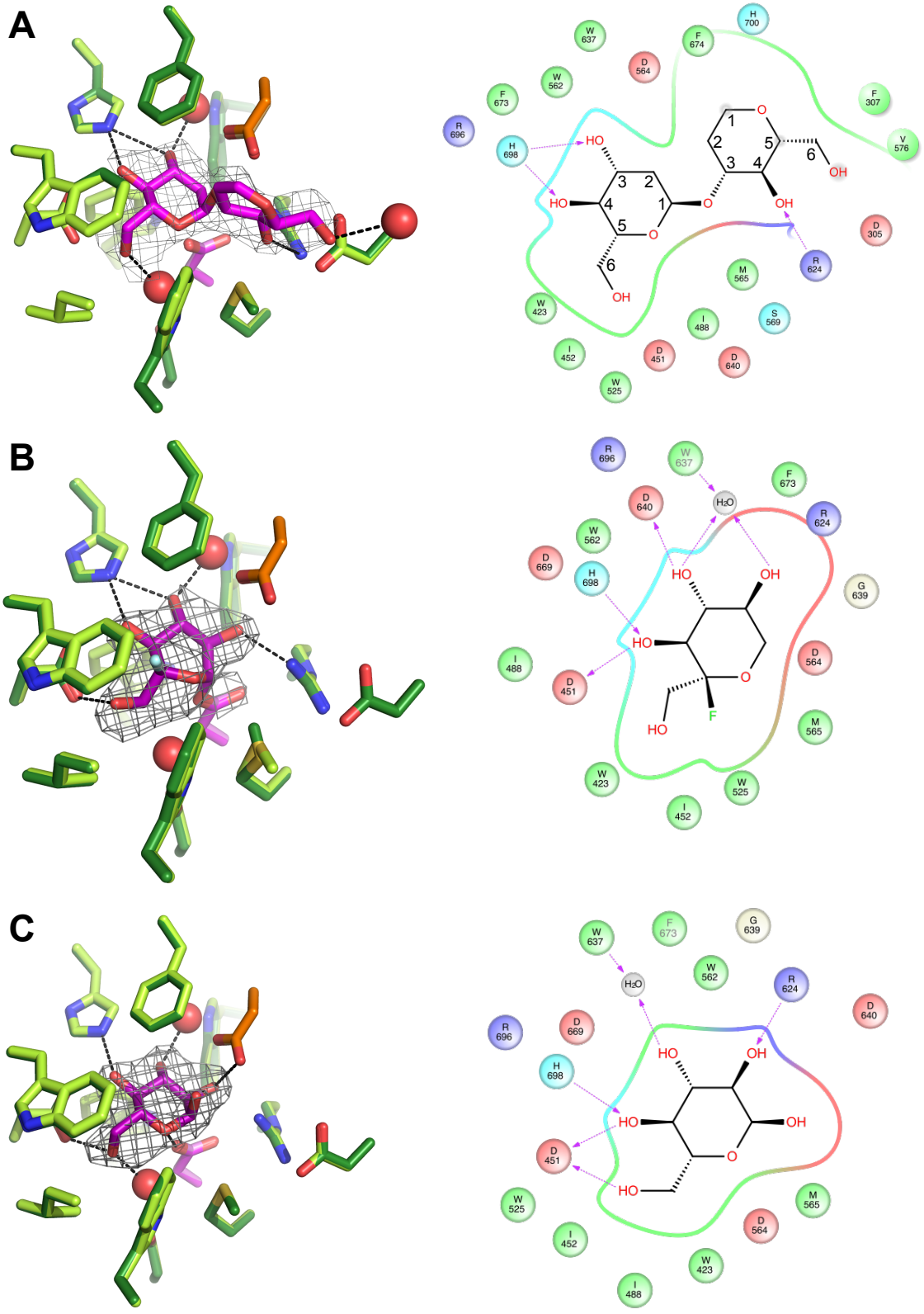

551

552 **Figure S7. Interactions of *Mm*α-GluII$_{Tryps}$ with its catalytic cycle ligands.** The *Mm*α-
553 GluII$_{Tryps}$ active site in crystals soaked with catalytic cycle ligands is represented with C-
554 atoms in dark green, and overlayed onto the apo structure with C-atoms in light green.
555 Unbiased F_o-F_c residual electron density maps are contoured at 3.0 σ. **(A)** D-Glucal
556 transglucosylation product, substrate analogue. (**B**) Adduct with 5-fluoro-D-glucose,
557 reaction intermediate analogue. (**C**) D-glucose, product. 2-Dimensional ligand plots made
558 with Maestro (35).
559

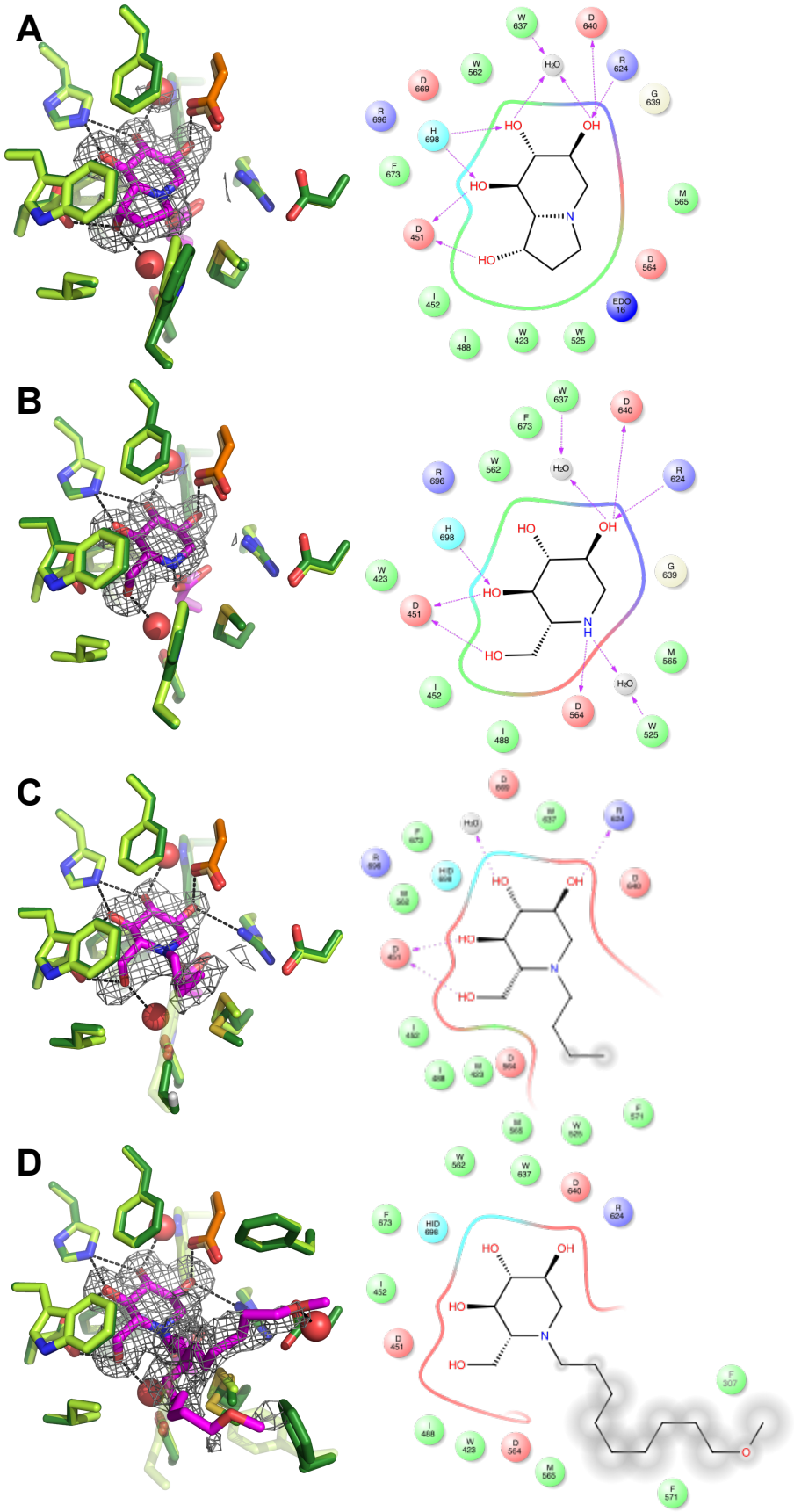
A
B
C
D

Figure S8. Interactions of *Mm*α-GluII$_{Tryps}$ with its iminosugar inhibitors. The *Mm* α -GluII$_{Tryps}$ active site in crystals soaked with inhibitors is represented with C-atoms in dark green, and overlayed onto the apo structure with C-atoms in light green. Unbiased F_o-F_c residual electron density maps are contoured at 3.0 σ. (**A**) Castanospermine. (**B**) DNJ. (**C**) *N*B-DNJ. The W525 apo structure side chain displaced by the inhibitor is in semi-transparent shaded representation (**D**) M*O*N-DNJ. The apo structure loop displaced by the inhibitor is in semi-transparent shaded representation. 2-Dimensional ligand plots made with Maestro(35).

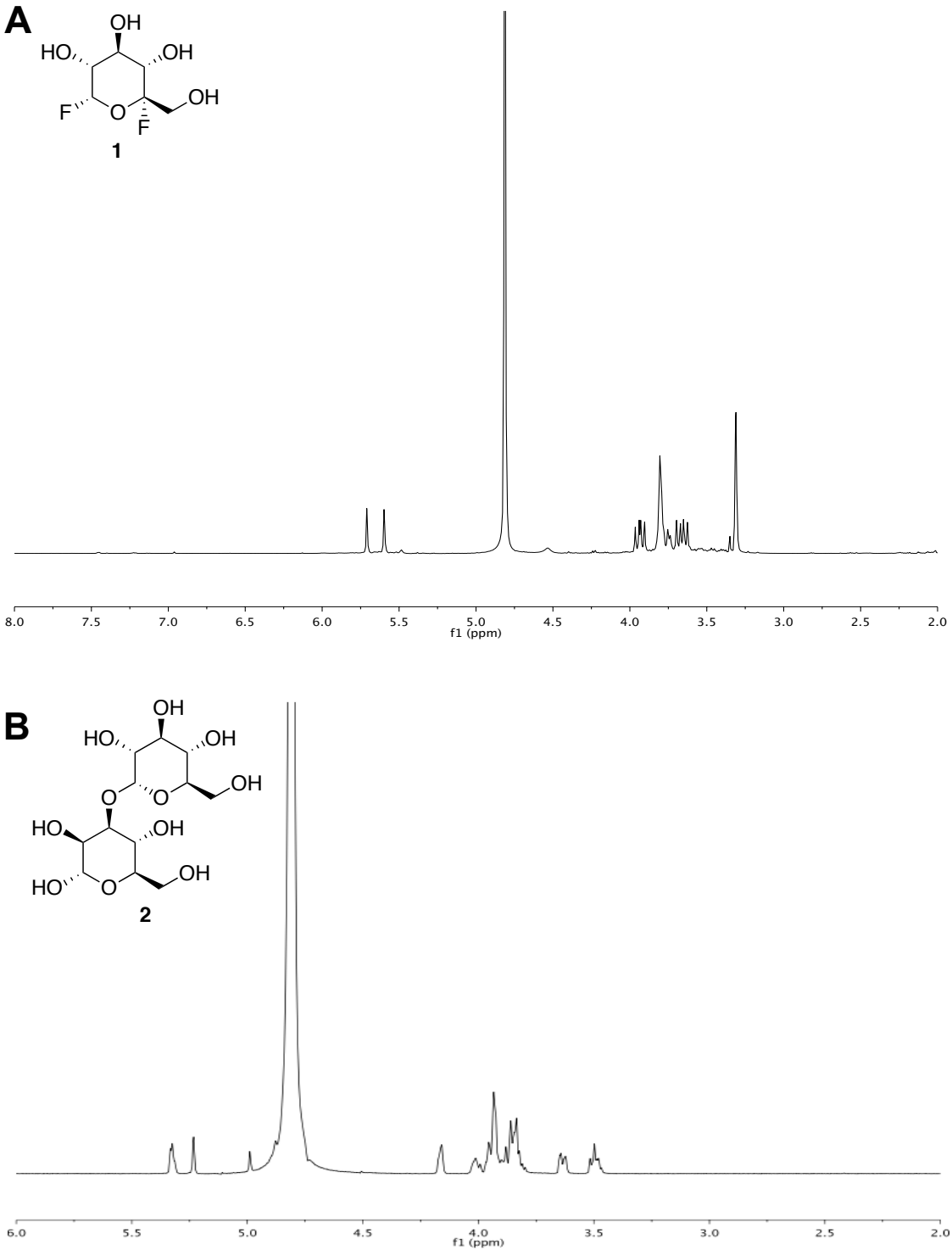

Figure S9. NMR spectra of 1. (**A**) ^{1}H NMR spectrum of **1** (500 MHz, CD_3OD). (**b**) ^{13}C NMR spectrum of **1** (125 MHz, CD_3OD). (**B**) ^{1}H NMR spectrum of **2** (500 MHz, CD_3OD)

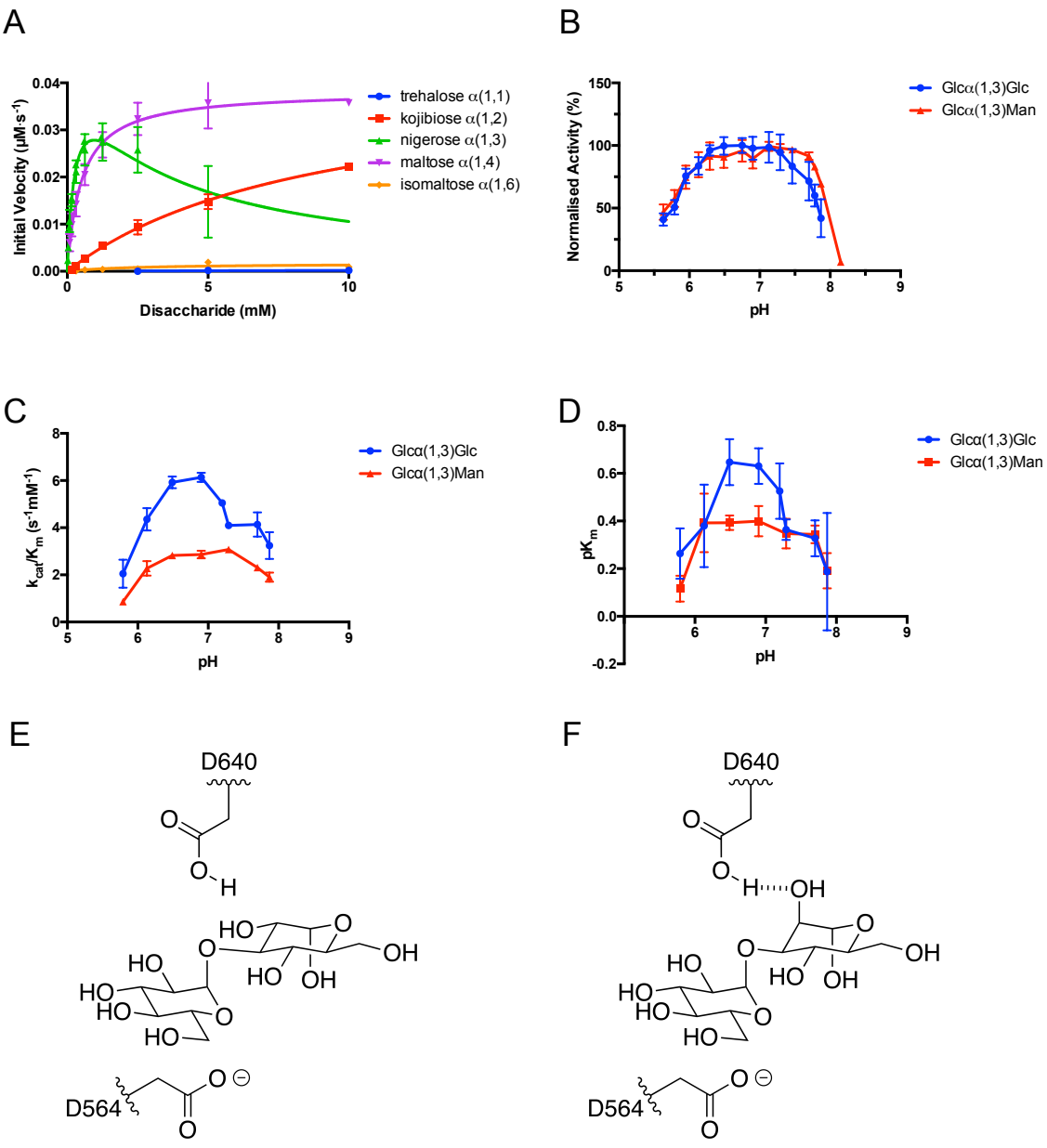

574

575 **Figure S10. α-GluII-mediated hydrolysis of disaccharides.** (**A**) *Mm*α-GluII activity

576 against a number of diglucosides. Michaelis-Menten curves for the different diglucosides

577 derived by non-linear regression analysis. The nigerose points are fitted to a substrate

578 inhibition model. (**B**) Normalized activity of Glc-α(1,3)-Glc and Glc-α (1,3)-Man

579 substrates over a range of pHs at 1mM substrate. (**C**) Plot of the specificity constant

580 k_{cat}/K_m over the same pH range as (**B**). (**D**) Plot of pK_m over the same pH range as (**B**).

581 Error bars are standard deviations from up to four separate experiments all conducted in
582 triplicate. (**E**) Schematic of Glc-α(1,3)-Glc binding between the two catalytic active site
583 residues. (**F**) Schematic of Glc-α(1,3)-Man binding between the two catalytic active site
584 residues, highlighting the proposed hydrogen bond donated by the general acid/base
585 D640 to the C-2 hydroxyl of the mannose ring at subsite +1.
586

Supplementary Tables.

Table S1. SAXS analysis of *Mm*α-GluII and *Mm*α-GluII$_{Tryps}$

	***Mm*α-GluII**	***Mm*α-GluII$_{Tryps}$**
***q* range, (nm^{-1})**	0.01-0.5	0.01-0.5
Exposure time (s)	10	10
Temperature (K)	293	293
Concentration Range, (mg ml^{-1})	0.17-2.97	0.13-4.12
Structural Parameters		
$I_{(0)}$ (cm^{-1}) [From P(r)]	159.10±0.59	74.80±0.16
Rg (nm) [from P(r)]	5.85±0.03	3.20±0.02
$I_{(0)}$ (cm^{-1}) [From Guinier]	157.84±0.89	74.70±0.12
Rg (nm) [from Guinier]	5.56±0.05	3.18±0.02
D_{max} (Å)	229	111
Porod Volume (nm^3)	293.83	166.68

Table S2. *Mm*α-GluII$_{Tryps}$ crystals. X-ray data collection and refinement statistics.

Structure, PDB ID	Apo, 5F0E	Glucal, 5HJO	5-Fl Glc fluoride, 5HJR	Glucose, 5H9O
Data collection				
Space group, Z	$P2_12_12$, 4	$P2_12_12_1$,8	$P2_1$,4	$P2_12_12_1$,8
Cell dimensions				
a,*b*,*c*(Å)	104.14,173.77,62.84	103.48,176.44,127.05	103.51,174.67,63.71	102.14,170.74,125.99
α, β, γ (°)	90.0, 90.0, 90.0	90.0, 90.0, 90.0	90.0, 91.31, 90.0	90.0, 90.0, 90.0
Resolution (Å)	59.09-1.74 (1.83-1.74)*	176.44-2.29 (2.41-2.29	174.66-2.40 (2.53-2.40)	87.66-2.37 (2.43-2.37)
R_{sym}	0.08 (0.64)	0.21 (1.57)	0.24 (2.46)	0.24(1.53)
I / sI	12.9 (2.4)	8.7 (1.1)	7.6 (1.2)	5.1(1.2)
$CC_{1/2}$	0.998 (0.802)	0.996 (0.562)	0.993 (0.376)	0.975(0.558)
Completeness (%)	94.7 (96.0)	96.9 (80.4)	99.3 (98.8)	99.7 (99.8)
Redundancy	3.9 (3.9)	6.5 (5.0)	6.9 (7.0)	5.5 (5.4)
Refinement				
Resolution (Å)	59.05-1.74	103.10-2.29	103.48-2.40	87.66-2.37
No. reflections	109901	101524	87211	89373
R_{work} / R_{free}	0.142/0.169	0.209/0.235	0.178/0.202	0.222/0.251
No. atoms				
Protein	8722	15035	15213	15268
Ligand/ion	309	420	175	381
Water	922	449	424	439
B-factors (Å^2)				
Protein	24.4	47.0	65.7	33.7
Ligand/ion	45.0	51.8	82.0	68.5
Water	35.3	42.3	48.7	25.8
R.m.s. deviations				
Bond lengths (Å)	0.01	0.01	0.01	0.01
Bond angles (°)	1.07	1.10	1.13	1.09
Ramachandran Plot (%)				
Favoured	97.8	97.7	97.8	97.7
Allowed	2.2	2.3	2.2	2.3
Forbidden	0	0	0	0

Each structure was determined with X-ray diffraction data coming from one crystal only.
Values in parentheses indicate data in the highest resolution shell.

Table S3. **Summary of activity and relative stability of *Mm*α-GluII, *Mm*α-GluII$_{Tryps}$ and the *Mm*α-GluII point mutants against different substrates.** S.E.M.: standard error of the mean.

	4-MUG			Glc2 Man7 GlcNAc2 -2AA	GlcMan7 GlcNAc2 -2AA	T_m (°C) (± S.E.M)
	Activity (% of wt)	**k_{cat} (s^{-1})**	**K_m (µM)**			
Mm α-GluII	YES	66.1 ± 3.8	10.0 ± 0.7	YES	YES	50.0 ± 0.5
Mm α-GluII$_{Tryps}$	70%	46.2 ± 5.0	10.5 ± 0.8	YES	YES	48.5 ± 0.1
D564N	NO	Not tested	Not tested	NO	NO	54.3 ± 0.1
D564E	NO	Not tested	Not tested	NO	NO	48.3 ± 0.1
D640N	NO	Not tested	Not tested	NO	NO	43.7 ± 0.2
F307G-ΔQ308	17%	Not tested	Not tested	Not tested	Not tested	46.3 ± 0.1
Δ307-308	NO	Not tested	Not tested	Not tested	Not tested	46.8 ± 0.2
R840E	10%	10.5±0.2	12.9± 1.0	Not tested	Not tested	43.3 ± 0.5

602 **Table S4. Kinetic parameters of diglucoside cleavage by *Mm*α-GluII.** Errors are the

603 95% confidence intervals§ based on five separate experiments.

Diglucoside, glycosidic bond	**V_{max} (nM/s)**	**k_{cat} (1/s)**	**K_m (mM)**	**k_{cat}/K_m (1/sM)**	**Goodness-of-fit, R^2**
Trehalose, α(1,1)	0.57	0.02 ± 0.06	19.09 ± 79.9	0.00	0.68
Kojibiose, α(1,2)	42.09	1.40 ± 0.07	8.98 ± 0.37	0.16	0.99
Nigerose, α(1,3)	45.14	1.50 ± 0.07	0.30 ± 0.08	5.05	0.99
Maltose, α(1,4)	38.3	1.28 ± 0.02	0.50 ± 0.03	2.54	0.99
Isomaltose, α(1,6)	1.67	0.06 ± 0.03	2.58 ± 3.65	0.02	0.56

604
605

606
607 **Table S5. *Mm*α-GluII$_{Tryps}$:iminosugar crystals. X-ray data collection and refinement**
608 **statistics.**
609

Structure, PDB ID	Castanospermine, 5IED	DNJ, 5IEE	*N*B-DNJ, 5IEF	M*O*N-DNJ, 5IEG
Data collection				
Space group, Z	$P2_12_12$, 4	$P2_12_12$,4	$P2_12_12$, 4	$P2_12_12$, 4
Cell dimensions				
a, *b*, *c* (Å)	103.4,173.9,63.0	103.48,173.71,62.91	103.84,172.89,62.77	104.32,173.31,63.03
α, β, γ (°)	90.0, 90.0, 90.0	90.0, 90.0, 90.0	90.0, 90.0, 90.0	90.0, 90.0, 90.0
Resolution (Å)	173.9-1.81 (1.91-1.81)*	88.9-1.92 (2.02-1.92)	103.84-2.38 (2.51-2.38)	104.32-1.82 (1.83-1.82)
R_{sym}	0.187 (1.726)	0.238 (1.605)	0.388 (1.957)	0.127(0.987)
$I / \sigma I$	8.8 (1.2)	7.2 (1.2)	5.6 (0.9)	12.1 (2.1)
$CC_{1/2}$	0.996 (0.476)	0.992 (0.412)	0.960 (0.396)	0.998(0.711)
Completeness (%)	100.0 (100.0)	100.0 (100.0)	95.9 (99.8)	100.0 (97.5)
Redundancy	6.7 (6.6)	6.6 (6.1)	4.9 (5.0)	6.7 (6.9)
Refinement				
Resolution (Å)	86.95-1.81	88.90-1.92	53.72-2.38	89.38-1.82
No. reflections	103735	87327	44118	102823
R_{work} / R_{free}	0.160/0.184	0.166/0.196	0.188/0.218	0.176/0.195
No. atoms				
Protein	7580	7577	7627	7562
Ligand/ion	213	196	152	163
Water	884	950	290	490
B-factors (Å^2)				
Protein	32.3	31.1	34.3	28.4
Ligand/ion	17.9	19.1	39.8	25.6
Water	43.1	41.6	63.3	28.7
R.m.s. deviations				
Bond lengths (Å)	0.01	0.01	0.01	0.01
Bond angles (°)	1.06	1.07	1.13	1.01
Ramachandran Plot (%)				
Favoured	97.2	97.2	96.8	96.9
Allowed	2.7	2.7	3.1	3.0
Forbidden	0	0	0.1	0.1

610
611
612

1. Alonzi DS, et al. (2013) Glycoprotein misfolding in the endoplasmic reticulum: identification of released oligosaccharides reveals a second ER-associated degradation pathway for Golgi-retrieved proteins. *Cell Mol Life Sci* 70(15):2799–2814.

2. Skelton BW, Stick RV, Stubbs KA, Watts AG, White AH (2004) The Fluorination (at C5) of Some Derivatives of D-Glucose. *Australian Journal of Chemistry* 57(4):345–353.

3. Praly J-P, Brard L, Descotes G, Toupet L (1989) Photohalogenation of glycopyranosyl halides: An expedient route to c-1 gem dihalogenated sugars. *Tetrahedron* 45(13):4141–4152.

4. Gottlieb HE, Kotlyar V, Nudelman A (1997) NMR Chemical Shifts of Common Laboratory Solvents as Trace Impurities. *J Org Chem* 62(21):7512–7515.

5. Boger DL, Honda T (1994) Total Synthesis of Bleomycin A2 and Related Agents. 4. Synthesis of the Disaccharide Subunit 2-O-(3-O-Carbamoyl-.alpha.-D-mannopyranosyl)-L-gulopyranose and Completion of the Total Synthesis of Bleomycin A2. *J Am Chem Soc* 116(13):5647–5656.

6. Vonrhein C, et al. (2011) Data processing and analysis with the autoPROC toolbox. *Acta Crystallogr D Biol Crystallogr* 67(Pt 4):293–302.

7. Winter G, Lobley CMC, Prince SM (2013) Decision making in xia2. *Acta Crystallogr D Biol Crystallogr* 69(Pt 7):1260–1273.

8. Kabsch W (2010) XDS. *Acta Crystallogr D Biol Crystallogr* 66(Pt 2):125–132.

9. Winn MD, et al. (2011) Overview of the CCP4 suite and current developments. *Acta Crystallogr D Biol Crystallogr* 67(Pt 4):235–242.

10. McCoy AJ, et al. (2007) Phaser crystallographic software. *J Appl Crystallogr* 40(Pt 4):658–674.

11. Keegan RM, Winn MD (2008) MrBUMP: an automated pipeline for molecular replacement. *Acta Crystallogr D Biol Crystallogr* 64(Pt 1):119–124.

12. Emsley P, Lohkamp B, Scott WG, Cowtan K (2010) Features and development of Coot. *Acta Crystallogr D Biol Crystallogr* 66(Pt 4):486–501.

13. Cowtan K (2006) The Buccaneer software for automated model building. 1. Tracing protein chains. *Acta Crystallogr D Biol Crystallogr* 62(Pt 9):1002–1011.

14. Blanc E, et al. (2004) Refinement of severely incomplete structures with maximum

likelihood in BUSTER-TNT. *Acta Crystallogr D Biol Crystallogr* 60(Pt 12 Pt 1):2210–2221.

15. Smart OS, et al. (2012) Exploiting structure similarity in refinement: automated NCS and target-structure restraints in BUSTER. *Acta Crystallogr D Biol Crystallogr* 68(Pt 4):368–380.

16. Chen VB, Wedell JR, Wenger RK, Ulrich EL, Markley JL (2015) MolProbity for the masses-of data. *J Biomol NMR* 63(1):77–83.

17. Brutus A, Sicilia F, Macone A, Cervone F, De Lorenzo G (2010) A domain swap approach reveals a role of the plant wall-associated kinase 1 (WAK1) as a receptor of oligogalacturonides. *Proc Natl Acad Sci USA* 107(20):9452–9457.

18. Batoko H, Zheng HQ, Hawes C, Moore I (2000) A rab1 GTPase is required for transport between the endoplasmic reticulum and golgi apparatus and for normal golgi movement in plants. *Plant Cell* 12(11):2201–2218.

19. Brandizzi F, et al. (2002) The destination for single-pass membrane proteins is influenced markedly by the length of the hydrophobic domain. *Plant Cell* 14(5):1077–1092.

20. Chinchilla D, et al. (2007) A flagellin-induced complex of the receptor FLS2 and BAK1 initiates plant defence. *Nature* 448(7152):497–500.

21. Petoukhov MV, et al. (2012) New developments in the ATSAS program package for small-angle scattering data analysis. *J Appl Crystallogr* 45(2):342–350.

22. Konarev PV, et al. (2003) PRIMUS: a Windows PC-based system for small-angle scattering data analysis. *J Appl Crystallogr* 36(5):1277–1282.

23. Svergun DI, IUCr (1992) Determination of the regularization parameter in indirect-transform methods using perceptual criteria. *J Appl Crystallogr* 25(4):495–503.

24. Svergun DI (1999) Restoring Low Resolution Structure of Biological Macromolecules from Solution Scattering Using Simulated Annealing. *Biophysical Journal* 76(6):2879–2886.

25. Volkov VV, Svergun DI, IUCr (2003) Uniqueness of ab initio shape determination in small-angle scattering. *J Appl Crystallogr* 36(3):860–864.

26. Kozin MB, Svergun DI, IUCr (2001) Automated matching of high- and low-resolution structural models. *J Appl Crystallogr* 34(1):33–41.

27. Pettersen EF, et al. (2004) UCSF Chimera--a visualization system for exploratory research and analysis. *J Comput Chem* 25(13):1605–1612.

28. Feng J, Romaniouk AV, Samal SK, Vijay IK (2004) Processing enzyme glucosidase II: proposed catalytic residues and developmental regulation during the ontogeny of the mouse mammary gland. *Glycobiology* 14(10):909–921.

29. Lu X, et al. (2009) Uncoupling of sustained MAMP receptor signaling from early outputs in an Arabidopsis endoplasmic reticulum glucosidase II allele. *Proc Natl Acad Sci USA* 106(52):22522–22527.

30. Stigliano ID, Alculumbre SG, Labriola CA, Parodi AJ, D'Alessio C (2011) Glucosidase II and N-glycan mannose content regulate the half-lives of monoglucosylated species in vivo. *Mol Biol Cell* 22(11):1810–1823.

31. Müller P, Köpke S, Sheldrick GM (2003) Is the bond-valence method able to identify metal atoms in protein structures? *Acta Crystallogr D Biol Crystallogr* 59(Pt 1):32–37.

32. Tamura K, et al. (2003) Why green fluorescent fusion proteins have not been observed in the vacuoles of higher plants. *Plant J* 35(4):545–555.

33. Ashkenazy H, Erez E, Martz E, Pupko T, Ben-Tal N (2010) ConSurf 2010: calculating evolutionary conservation in sequence and structure of proteins and nucleic acids. *Nucleic Acids Res* 38(Web Server issue):W529–33.

34. Robert X, Gouet P (2014) Deciphering key features in protein structures with the new ENDscript server. *Nucleic Acids Res* 42(Web Server issue):W320–4.

35. Schrodinger, LLC (2015) Maestro.